AIAA 99–1467

LOW ORDER AERODYNAMIC MODELS FOR AEROELASTIC CONTROL OF TURBOMACHINES

K.E. Willcox, J.D. Paduano, J. Peraire,
Massachusetts Institute of Technology
Cambridge, MA
K.C. Hall
Duke University
Durham, NC

40th AIAA/ASME/ASCE/AHS/ASC Structures, Structural Dynamics and Materials (SDM) Conference
April 12-15, 1999
St Louis, MO

LOW ORDER AERODYNAMIC MODELS FOR AEROELASTIC CONTROL OF TURBOMACHINES

K.E. Willcox[*], J.D. Paduano[†], J. Peraire[‡]
Massachusetts Institute of Technology
Cambridge, MA
K.C. Hall[§]
Duke University
Durham, NC

Abstract

A reduced order aerodynamic model is developed for aeroelastic analysis of turbomachines. The proper orthogonal decompostion technique is used to obtain the modal basis vectors of this model. Two-dimensional frequency domain solutions are used to obtain the basis vectors efficiently, however the model itself is developed in the time domain and is cast in state-space form. The number of states of the model is less than ten per blade passage, making it appropriate for control applications. The aerodynamic model is coupled with a simple structural model that has two degrees of freedom for each blade. Results are presented for unsteady inviscid flow through a single stage rotor that moves in both pitch and plunge. The technique is applicable to viscous and three-dimensional problems as well as multi-stage problems with inlet and exit disturbance flows.

Introduction

With the current trend towards increased operating speeds and more flexible blading, aeroelasticity has become a critical consideration in the design of compressors. Understanding and predicting aeroelastic phenomena are crucial to ensuring that a compressor will operate within stability boundaries, and thus has a large impact on the design process. Appropriate blade design, together with strategies for controlling the onset of instabilities, can significantly impact the stable operating range, potentially leading to better compressor performance. In addition, understanding high cycle fatigue is important to prolong engine lifetimes.

[*]Research Assistant, Department of Aeronautics and Astronautics

[†]Principal Research Engineer, Department of Aeronautics and Astronautics

[‡]Associate Professor, Department of Aeronautics and Astronautics

[§]Associate Professor, Department of Mechanical Engineering and Materials Science. Associate Fellow AIAA

Various possible flow control methods for extending the stable operating range of compressors are currently under investigation. For *active* control, a variety of actuation mechanisms could be employed, including air injection and piezo-electrics. Implementation of these actuators with the appropriate control law would be used to ensure that blade vibrations remain damped. It is also possible to extend the stability boundaries of the compressor by altering the aerodynamic or structural properties of the blades. Mistuning is an example of this approach : rotor symmetry is broken by making the blades different from one another, either structurally or aerodynamically, and thus introducing a distribution of blade frequencies in the cascade.[1] Experimental and numerical results show that intentional mistuning of rotor blades can delay the onset of instabilities.[2] Mistuning is a form of *passive* control for flutter or high cycle fatigue.

Aeroelastic phenomena involve a complicated interaction between the aerodynamics and the structural dynamics of the blades. Typically, very simple aerodynamic models have been used for aeroelastic analyses. The flow is usually assumed to be two-dimensional, inviscid and incompressible.[3] These methods are useful near design conditions but do not predict the flow well off-design where blade loading effects are important.[4] They are also not applicable to transonic flows where shock dynamics play a significant role in determining the aerodynamic response. The non-linear problem can be solved using computational fluid dynamics (CFD) methods to perform simulations of the unsteady Euler or Navier-Stokes equations, however such techniques are computationally very expensive and have a large number of degrees of freedom, which means that they are not suitable for control design purposes. More efficient methods for time-varying flow can be obtained by considering the unsteady solution to be a small perturbation about a steady-state flow.[5] A set of linearised equations is then obtained which can be time-marched to obtain a flow solution at each instant. This approach is still computationally very expensive and is not really practicable for analysis of a full rotor. If the flow disturbances are assumed to be harmonic in time, the linearised governing equations can then be cast in the frequency domain. Further simplifications can be obtained by decomposing the disturbances into circumferential frequency components. A complex phase shift condition can then be enforced, so that only one blade passage of the rotor need be considered for any analysis in which all rotor blades are the same. For a mistuning problem however, the full rotor must still be considered. Even with these simplifications, for control applications the number of states is still prohibitively high.

The aim of this research is to develop a framework for the prediction and control of aeroelastic effects. Such a tool requires a sophisticated aerodynamic model which can capture important unsteady flow features, including transonic flows where shocks are present. In some problems, viscous effects or non-linearity may be crucial, therefore the framework must allow inclusion of these effects. From a control perspective, we require that the model has a low number of states and takes an input/output form. For active flow control, a model of the actuation mechanism must also be included.

Reduced order models for turbomachinery problems have previously been developed in the frequency domain.[6] In this research, an aerodynamic low order model will be developed in the time domain using the proper orthogonal decomposition (POD) technique.[7] The technique will be presented for two-dimensional problems, but the extension to three dimensions is straightforward. The frequency domain will be used to construct the POD modes efficiently. The model will be cast in state-space form with an expected size of less than ten states per blade passage for each degree of freedom (pitch and plunge) for the two-dimensional case. Derivation of time-domain models is a crucial first step for many control-theoretic design and analysis approaches. It also enables the aerodynamics to be easily incorporated within a global engine model or coupled to an actuation model. The tractable size of the model makes it amenable to control design. It also allows for many blade passages to be considered and for the analysis of multi-stage problems.

In this paper the framework for developing these models is described. Possible uses of the model are design of active control strategies or analysis of a mistuned rotor. Here, as an illustration, the aerodynamic low order model is coupled with a simple blade structural model and the coupled system behaviour investigated. Results for unsteady inviscid flow through a single rotor stage are presented. The technique is readily extended to include multi-stage and three-dimensional analyses and viscous effects. Upstream duct and downstream plenum models could also be incorporated for analysis of the effects of inlet distortion. Extensions to the basic model will be discussed in future papers.

Computational Model

Non-Linear Model

Consider an arbitrary two-dimensional time-varying control volume $\Omega(t)$, with boundary $\Gamma(t)$. The Euler equations governing the unsteady two-dimensional flow of an inviscid compressible fluid can be written in integral form as

$$\frac{\partial}{\partial t}\int_{\Omega} U\,dxdy + \oint_{\Gamma}\left(Fn_x + Gn_y\right)d\Gamma = 0 \qquad (1)$$

where n_x and n_y are unit vectors pointing out of Ω, U is the unknown vector of conserved variables given by

$$U = (\rho, \rho u, \rho v, e)^T \qquad (2)$$

and F and G are the inviscid flux vectors given by

$$F = \begin{pmatrix} \rho(u - x_t) \\ p + \rho u(u - x_t) \\ \rho v(u - x_t) \\ pu + e(u - x_t) \end{pmatrix}$$
$$G = \begin{pmatrix} \rho(v - y_t) \\ \rho u(v - y_t) \\ p + \rho v(v - y_t) \\ pv + e(v - y_t) \end{pmatrix}. \qquad (3)$$

Here ρ, u, v, p and e denote density, cartesian velocity components, pressure and total energy respectively. x_t and y_t are the speeds in the x and y directions with which the boundary $\Gamma(t)$ moves. Also, for an ideal gas the equation of state becomes

$$e = \frac{p}{\gamma - 1} + \frac{1}{2}\rho(u^2 + v^2). \qquad (4)$$

The governing equations are discretised using a finite volume formulation on an unstructured triangular grid covering the computational domain and approximations to the unknown flow vector U are sought at the vertices of that grid. For a vertex j, equation (1) can be written

$$\frac{d}{dt}\left(V_j U_j\right) + \int_{\Gamma_j}(Fn_x + Gn_y)d\Gamma = 0, \qquad (5)$$

where V_j is the volume consisting of all the triangles having vertex j, Γ_j is the boundary of V_j and U_j represents the average value of U over volume V_j. The integral in equation (5) is evaluated by considering weighted summations of flux differences across each edge in the control volume.[8] This leads to a large set of non-linear ordinary differential equations which can be written as

$$\frac{d\mathbf{U}}{dt} + R(\mathbf{U}, \mathbf{x}) = 0, \qquad (6)$$

where now $\mathbf{U}$ is the global vector of unknowns at each node and $R(\mathbf{U},\mathbf{x})$ represents the non-linear flux contributions which are a function of both the problem geometry $\mathbf{x}$ and the flow solution $\mathbf{U}$. Appropriate boundary conditions must be applied at the surfaces of the blades and at farfield boundaries. To obtain a rectilinear two-dimensional representation of the cascade, the rotor is unwrapped in the circumferential direction as shown in figure 1. The boundaries extending upstream from the leading edge and downstream from the trailing edge of the top and bottom blade surfaces are periodic boundaries. The condition that the flow along the upper periodic boundary is the same as that along the lower periodic boundary is enforced.

Steady-state solutions can be evaluated by driving the non-linear residual $R(\mathbf{U},\mathbf{x})$ to zero. This is done by implementation of a Newton scheme coupled with an iterative GMRES solver.[9] Assuming subsonic axial conditions, the density, total enthalpy and tangential velocity are prescribed at the inlet boundary and the exit pressure is specified. At the blade surfaces, a flow tangency condition is applied to the velocity. For steady-state flows in which the solution is the same in all passages, the computation can be performed on a single blade passage with use of the periodic boundary conditions described above.

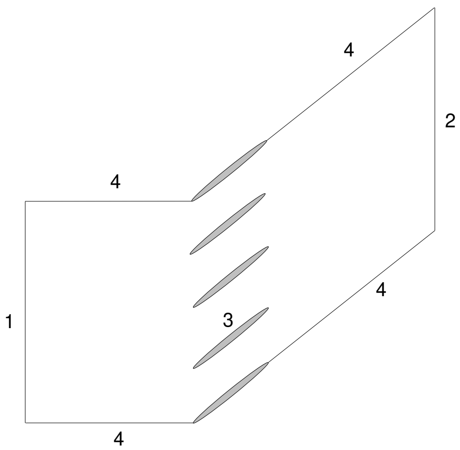

Fig. 1 Rectilinear two-dimensional representation of cascade. Inlet boundary (1), exit boundary (2), blade surfaces (3) and periodic boundaries (4).

Linearised Model

For consideration of unsteady flows, caused by unsteady disturbances in the passage or by blade motion, the full non-linear equation (6) could be integrated in time. This procedure is computationally expensive, especially if the disturbances considered have circumferential variation. If we limit ourselves to the consideration of small amplitude unsteady motions, the problem can be considerably simplified by linearising the equations. We assume that the unsteady solution is a small perturbation about a steady-state flow and that the grid motion is a small variation about the steady-state grid

$$\mathbf{U}(\mathbf{x},t) = \overline{\mathbf{U}}(\mathbf{x}) + \mathbf{U}'(\mathbf{x},t) \quad \mathbf{x}(t) = \overline{\mathbf{x}} + \mathbf{x}'(t). \tag{7}$$

Performing a Taylor expansion about $\overline{\mathbf{U}}$ and $\overline{\mathbf{x}}$ of the non-linear term $R(\mathbf{U},\mathbf{x})$ in equation (6) we obtain

$$R(\mathbf{U},\mathbf{x}) \simeq R(\overline{\mathbf{U}},\overline{\mathbf{x}}) + \frac{\partial R}{\partial \mathbf{U}}(\overline{\mathbf{U}},\overline{\mathbf{x}})\mathbf{U}' + \frac{\partial R}{\partial \mathbf{x}}(\overline{\mathbf{U}},\overline{\mathbf{x}})\Delta\mathbf{x}. \tag{8}$$

Using the fact that $R(\overline{\mathbf{U}},\overline{\mathbf{x}}) = 0$ and assuming that the perturbations are small so that quadratic and higher order terms in $\mathbf{U}'$ and $\Delta\mathbf{x}$ can be neglected, the linearised form of equation (6) is

$$\frac{d\mathbf{U}'}{dt} + A\mathbf{U}' = -\frac{\partial R}{\partial \mathbf{x}}\Delta\mathbf{x}, \tag{9}$$

where A is the tangent matrix $\frac{\partial R}{\partial \mathbf{U}}$ evaluated at steady-state conditions. Note that due to the linear assumption, the grid is not actually deformed for unsteady calculations, however the term on the righthand side of equation (9) represents the first order effects of grid motion.

Boundary conditions are applied according to the unsteady perturbations present in the flow. The velocity on the blade surfaces is set equal to the normal component of velocity induced by blade motions. At farfield boundaries, the incoming one-dimensional characteristic quantities are evaluated in terms of perturbations in the inlet and exit flows as follows. At the inlet prescribe entropy, vorticity and downstream running pressure waves which are given respectively by

$$\begin{aligned} c_1 &= p' - \overline{c}^2\rho' \\ c_2 &= \overline{\rho}\ \overline{c}\ u_t' \\ c_3 &= p' - \overline{\rho}\ \overline{c}\ u_n'. \end{aligned} \tag{10}$$

At the outflow boundary prescribe the upstream running pressure wave given by

$$c_3 = p' - \overline{\rho}\ \overline{c}\ u_n'. \tag{11}$$

Here, u_n' and u_t' are the normal and tangential components of perturbation velocity, and $\overline{c}$ is the speed of sound of the steady-state flow. It is also possible to use more sophisticated models for the inlet and exit boundary conditions.[10]

Reduced Order Aerodynamic Model

Reduced Order Representation of Flow Solution

The idea behind developing a reduced order aerodynamic model is to construct a set of orthogonal basis functions which span the solution space efficiently. If the flow is assumed to be a linear combination of these basis vectors, then the large set of ordinary differential equations (9) can be reduced to a much smaller system.

The perturbation solution $\mathbf{U}'$ is considered to comprise two parts - the homogeneous portion which satisfies homogeneous boundary conditions and the inhomogeneous part which satisfies the non-zero boundary conditions. These conditions could be on blade position and motion, or on disturbances at the passage inlet and exit. We consider here a model in which the blade can move in pitch and plunge but the perturbation characteristic quantities at the inlet and exit are prescribed to be zero. The results developed here for models with blade motion only are easily extended to include problems with inflow and outflow disturbances.

We can decompose the solution at any time t into a homogeneous portion and components due to the pitching and plunging motion of the blade

$$\mathbf{U}'(\mathbf{x},t) = \mathbf{U}_{hom}(\mathbf{x},t) + h(t)\mathbf{U}_h(\mathbf{x}) + \dot{h}(t)\mathbf{U}_{\dot{h}}(\mathbf{x}) + \alpha(t)\mathbf{U}_\alpha(\mathbf{x}) + \dot{\alpha}(t)\mathbf{U}_{\dot{\alpha}}(\mathbf{x}). \quad (12)$$

The homogeneous part of the solution is assumed to be a linear combination of the first m basis functions

$$\mathbf{U}_{hom}(\mathbf{x},t) = \sum_{i=1}^{m} a_i(t)\mathbf{\Psi}_i(\mathbf{x}), \quad (13)$$

where m is much smaller than the number of unknowns in the vector $\mathbf{U}'$. The non-homogeneous functions $\mathbf{U}_h$, $\mathbf{U}_{\dot{h}}$, $\mathbf{U}_\alpha$ and $\mathbf{U}_{\dot{\alpha}}$ are particular solutions of the flow system and are precomputed by solving for steady flows with unit boundary conditions on blade position and velocity.

Determination of Basis Functions

The proper orthogonal decomposition (POD)[7] is used to compute an efficient orthogonal basis. Denote the scalar product of two vectors x and y by (x, y) and define a time averaging operation on x as $\langle x \rangle$. We wish to seek a set of functions which represent the solution $\mathbf{U}(\mathbf{x},t)$ in an optimal way. This can be written

$$\max_{\mathbf{\Phi}} \frac{\langle |(\mathbf{U},\mathbf{\Phi})|^2 \rangle}{(\mathbf{\Phi},\mathbf{\Phi})} = \frac{\langle |(\mathbf{U},\mathbf{\Psi})|^2 \rangle}{(\mathbf{\Psi},\mathbf{\Psi})}, \quad (14)$$

where $\mathbf{\Psi}$ is the function which maximises the norm of the scalar product with the field $\mathbf{U}(\mathbf{x},t)$. It can be shown that a necessary condition for (14) to hold is that $\mathbf{\Psi}$ is an eigenfunction of the kernel K defined by

$$K(x,x') = \frac{1}{n}\sum_{i=1}^{n} \mathbf{U}_i(x)\mathbf{U}_i(x'), \quad (15)$$

where $\mathbf{U}_i(\mathbf{x})$ is the instantaneous flow field at a time t_i and the number of snapshots n is sufficiently large.[11] The eigenvectors of K are of the form

$$\mathbf{\Psi} = \sum_{i=1}^{n} B_i\mathbf{U}_i, \quad (16)$$

where the constants B_i can be seen to satisfy the eigenvector equation

$$CB = \Lambda B \quad (17)$$

and C is now the correlation matrix

$$C_{ij} = \frac{1}{n}(\mathbf{U}_i, \mathbf{U}_j). \quad (18)$$

It can also be shown that the maximum in (14) is achieved and the eigenfunction obtained corresponds to λ_1, the largest eigenvalue of C.[11] We compute all the eigenmodes of the correlation matrix and order them according to the size of the eigenvalue $\lambda_1 > \lambda_2 > ... > \lambda_n$. Then for any k we represent the solution as a linear combination of basis functions

$$\mathbf{U}(\mathbf{x},t) = \sum_{i=1}^{k} a_i(t)\mathbf{\Psi}_i(\mathbf{x}), \quad (19)$$

where

$$\sum_{i=1}^{k}\langle |a_i(t)|^2 \rangle = \sum_{i=1}^{k}\lambda_i \quad (20)$$

and for a given number of modes the POD is optimal for reconstructing a signal $\mathbf{U}(\mathbf{x},t)$ in the sense that it contains the greatest possible amount of average "kinetic energy" $\langle(\mathbf{U},\mathbf{U})\rangle$.

Typically in a POD analysis of this form the snapshots would be obtained from a full time-marching simulation code. For general perturbations however, the entire rotor must be included in the analysis, therefore making the calculations expensive. A more convenient approach is to use linearity and the frequency domain to obtain snapshots more efficiently. Due to the linear nature of the governing equations (9), any general farfield disturbance or blade motion can be decomposed into a summation of travelling wave modes containing just a single spatial frequency σ and a single temporal frequency ω. The spatial modes can be thought of as eigenmodes whose shapes are Fourier modes in the circumferential direction.[12] Due to the discrete nature of the blades, any general motion of the rotor blades will consist of a finite number of spatial Fourier modes. For a rotor with N blades, there are N modes which may be present in the blade motion, with spatial frequencies given by

$$\sigma_j = \frac{(j-1)2\pi}{N} \qquad j = 1, 2, ..., N. \quad (21)$$

Here, σ_j is the interblade phase angle and describes the phase difference between the motion of a given blade and its neighbour.[5] For inlet and exit disturbance flows which have a continuous circumferential variation, the possible spatial frequency components are not restricted to these discrete values.

If the forcing is assumed to be

$$\mathbf{f}(\mathbf{x},t) = \overline{\mathbf{f}}(\mathbf{x})e^{i\omega t}, \quad (22)$$

then the time variation of the flow can be assumed to be harmonic of the form

$$\mathbf{U}'(\mathbf{x},t) = \overline{\mathbf{U}}(\mathbf{x})e^{i\omega t}, \quad (23)$$

where $\overline{\mathbf{U}}(\mathbf{x})$ and $\overline{\mathbf{f}}(\mathbf{x})$ are complex magnitude vectors. The linearised Euler equations (9) then become

$$[A + i\omega]\overline{\mathbf{U}} = \overline{\mathbf{f}}. \tag{24}$$

The complex solution $\overline{\mathbf{U}}(\mathbf{x})$ can be obtained from a single solution of (24) for each temporal frequency ω.

Since the equations are cast in the frequency domain, and the problem has been formualated so as to contain a single spatial frequency, advantage can now be taken of a complex periodicity relationship to reduce the required size of the computational domain to a single blade passage. For any given spatial frequency σ, only one passage needs to be considered, with the periodicity condition now that the flow along the upper periodic boundary is the same as that along the lower periodic boundary but shifted by the interblade phase angle. This can be written

$$\overline{\mathbf{U}}(x, y+G) = \overline{\mathbf{U}}(x,y)e^{i\sigma}, \tag{25}$$

where G is the spacing between rotor blades. Additionally we note that solutions for flows with different interblade phase angles are orthogonal to one another.

Conventional POD analysis on a purely sinusoidal response shows that only two independent modes exist for each frequency. Rather than obtaining the snapshots in the time domain, we instead solve the frequency domain system (24) at a set of sample frequencies and take the real and imaginary parts of each complex solution $\overline{\mathbf{U}}$ as snapshots. If the complex single passage solution for interblade phase angle σ has real and imaginary parts $\overline{\mathbf{U}}_R$ and $\overline{\mathbf{U}}_I$ respectively, the snapshots are constructed as follows

$$\mathbf{U}_1 = \begin{bmatrix} \overline{\mathbf{U}}_R \\ \overline{\mathbf{U}}_R cos\sigma - \overline{\mathbf{U}}_I sin\sigma \\ \overline{\mathbf{U}}_R cos2\sigma - \overline{\mathbf{U}}_I sin2\sigma \\ \cdots \\ \overline{\mathbf{U}}_R cos(N-1)\sigma - \overline{\mathbf{U}}_I sin(N-1)\sigma \end{bmatrix} \tag{26}$$

and

$$\mathbf{U}_2 = \begin{bmatrix} \overline{\mathbf{U}}_I \\ \overline{\mathbf{U}}_I cos\sigma + \overline{\mathbf{U}}_R sin\sigma \\ \overline{\mathbf{U}}_I cos2\sigma + \overline{\mathbf{U}}_R sin2\sigma \\ \cdots \\ \overline{\mathbf{U}}_I cos(N-1)\sigma + \overline{\mathbf{U}}_R sin(N-1)\sigma \end{bmatrix}, \tag{27}$$

where N is the number of blade passages in the rotor. The non-homogeneous part of these snapshots is extracted by subtracting the appropriate amount of the correction functions $\mathbf{U}_h$, $\mathbf{U}_{\dot{h}}$, $\mathbf{U}_\alpha$ and $\mathbf{U}_{\dot{\alpha}}$. The modes $\mathbf{\Psi}$ obtained from the POD analysis therefore satisfy homogeneous boundary conditions.

The unsteadiness of the motion can be characterised by the reduced frequency k which is defined as

$$k = \frac{\omega c}{V}, \tag{28}$$

where ω is the frequency of the sinusoidal motion, c is the blade chord and V is the farfield inlet velocity. A set of sample frequencies are selected at which snapshots are obtained. It is important to ensure that the range sampled includes all important frequencies in problems of interest. It is also necessary to ensure that enough samples are made over the given range. These issues will be further discussed in the results section.

Construction of Low Order Model

Although the modes are computed using analysis of a single passage in the frequency domain to obtain the snapshots, the low order model is developed in the time domain. It is therefore necessary to consider all N blade passages to enforce the periodicity condition.

Substituting the expansions (12) and (13) into the governing equations (9) and using orthogonality, a system of ordinary differential equations for the modal coefficients is obtained as follows

$$\frac{da_i}{dt} + \mathbf{\Psi}_i^T A \sum_j a_j \mathbf{\Psi}_j = f_i, \tag{29}$$

where the forcing vector $\mathbf{f}$ is given by

$$f_i(t) = -\dot{h}(t)\mathbf{\Psi}_i^T\mathbf{U}_h - \ddot{h}(t)\mathbf{\Psi}_i^T\mathbf{U}_{\dot{h}} - \dot{\alpha}(t)\mathbf{\Psi}_i^T\mathbf{U}_\alpha - \ddot{\alpha}(t)\mathbf{\Psi}_i^T\mathbf{U}_{\dot{\alpha}}. \tag{30}$$

The system of equations (29) can be written equivalently in state-space form. As noted previously, two flow solutions at differing interblade phase angles are orthogonal to one another, so the equation systems for each value of σ are decoupled. For interblade phase angle σ we can write

$$\dot{\mathbf{z}}_\sigma = \mathcal{A}_\sigma \mathbf{z}_\sigma + \mathcal{B}_\sigma \mathbf{u}_\sigma, \tag{31}$$

where $\mathbf{z}_\sigma$ is the state vector containing the modal coefficients a_j for those modes corresponding to interblade phase angle σ. The input vector $\mathbf{u}_\sigma$ contains the magnitude of the component of blade position, velocity and acceleration corresponding to interblade phase angle σ. Rather than specifying blade motion in terms of interblade phase angle components, we would like to be able to specify the actual positions, velocities and accelerations of each blade as a function of time. The problem is formulated in a standing wave representation which allows for arbitrary transient motion of the blades.[13] The arbitrary motion of N blades h_j can be represented as a superposition of N standing wave modes

$$h_j(t) = \sum_{r=0}^{\frac{N-1}{2}} \left[h_{cr}(t)cos(j\sigma_r) + h_{sr}(t)sin(j\sigma_r)\right]. \tag{32}$$

This can be written equivalently in matrix form as

$$\mathbf{u} = P\mathbf{v}, \tag{33}$$

where $\mathbf{u}$ contains the positions, velocities and accelerations of each blade as a function of time and $\mathbf{v}$ contains the so-called multiblade coordinates h_{cr} and h_{sr}. The full state-space system then becomes

$$\dot{\mathbf{z}} = \mathcal{A}\mathbf{z} + \mathcal{B}\mathbf{u} \qquad \mathbf{y} = \mathcal{C}\mathbf{z} + \mathcal{D}\mathbf{u}, \tag{34}$$

where $\mathbf{z}$ now contains all the modal coefficients. The $\mathcal{A}$ matrix is block diagonal according to interblade phase angle, but the $\mathcal{B}$ matrix is now fully populated and couples the system. The output vector $\mathbf{y}$ contains quantities of interest, usually the forces and moments on each blade as a function of time.

Results

Aerodynamic Low Order Model for Transonic Cascade

Low order models have been developed for subsonic and transonic cascades operating at any interblade phase angle. A DFVLR L030-4 transonic rotor which operates at a steady-state Mach number of 0.82 was analysed in unsteady plunging motion for a four blade configuration. Figure 2 shows the grid for this rotor. The steady state solution is shown in figure 3.

Fourteen snapshots were obtained for each interblade phase angle, with samples being made at reduced frequencies of 0.18, 0.37, 0.55, 0.74, 0.92, 1.85 and 2.77. The POD eigenvalue spectra are plotted in figures 4 and 5 for interblade phase angles of 0°, 180° and ±90°. These plots show that most of the flow energy is captured within the first six or eight modes for each interblade phase angle. Note that due to the standing mode formulation, snapshots for 90° and −90° are included together in the POD analysis.

The eigenvalues of the low order system were computed and are shown in figure 6. Each eigenvalue is identified with the interblade phase angle to which it corresponds. We see that there is a number of lightly damped modes for the ±90° case. The eigenvalues fall into two main regions. There is the small cluster of values near the real axis around -8. These are in fact the first mode for each interblade phase angle and correspond to a time delay or inertial lag in the aerodynamic system. The other eigenvalues form an almost vertical line nearer the origin. It is thought that this line could be a discrete representation of a branch cut.[14]

One question which must be addressed is that of choosing the sample frequencies. It is necessary to ensure that the appropriate range of frequencies is sampled, and also that sufficient samples are taken over this range. Forced response of the cascade to a pulse input is a good way of assessing this, since a pulse contains a continuous spectrum of frequencies as well as all possible interblade phase angles. Comparison of low order model results with the full simulation code will determine whether enough sample frequencies were used to construct the POD basis vectors. The input takes the form

$$h(t) = he^{-g(t-t_0)^2}, \tag{35}$$

where g is a parameter which determines how sharp the pulse is and thus the value of the highest significant frequency present.

Firstly, all four blades were supplied with the same input. This results in a motion in which only an interblade phase angle of zero is present and which can be solved using the linearised simulation code with just a single passage. The blade position input and non-dimensional lift force response as a function of time are depicted in figures 7 and 8. It shows that very good agreement is obtained with only four or six modes in the low order model. A case was then considered where just one blade was forced with the pulse input, while the other three were held fixed. This motion contains all possible interblade phase angles. The inputs and response for each blade computed using the low order model with six modes per interblade phase angle are shown in figure 9. The linearised simulation code would require solving the large system (9) over the full four-passage domain. A computation of this size was found to be impractical.

Structural Coupling

A simple two degree of freedom structural model for each blade as shown in figure 10 was coupled to the aerodynamic low order model. The structural equations of motion can be written in non-dimensional form

$$\begin{bmatrix} M_1 & 0 & . & . & 0 \\ 0 & M_2 & 0 & . & 0 \\ . & . & . & . & . \\ . & . & . & . & . \\ 0 & . & . & 0 & M_N \end{bmatrix} \begin{Bmatrix} \ddot{q}_1 \\ \ddot{q}_2 \\ . \\ . \\ \ddot{q}_N \end{Bmatrix} + \begin{bmatrix} K_1 & 0 & . & . & 0 \\ 0 & K_2 & 0 & . & 0 \\ . & . & . & . & . \\ . & . & . & . & . \\ 0 & . & . & 0 & K_N \end{bmatrix} \begin{Bmatrix} q_1 \\ q_2 \\ . \\ . \\ q_N \end{Bmatrix} = \begin{Bmatrix} F_1 \\ F_2 \\ . \\ . \\ F_N \end{Bmatrix}, \tag{36}$$

where $[M_i]$ and $[K_i]$ are the non-dimensional mass and stiffness matrices for each blade i and are given by

$$[M_i] = \begin{bmatrix} 1 & x_\alpha \\ x_\alpha & r_\alpha^2 \end{bmatrix}_i \qquad [K_i] = \begin{bmatrix} \left(\frac{\omega_h}{\omega_\alpha}\right)^2 & 0 \\ 0 & r_\alpha^2 \end{bmatrix}_i. \tag{37}$$

Here ω_h and ω_α are the uncoupled natural frequencies of the blade in plunge and pitch respectively, $S_\alpha = mbx_\alpha$ is the static unbalance and $I = mb^2r_\alpha^2$ is the section moment of inertia about the elastic axis. The load and displacement vectors for each blade are

$$\{F_i\} = \frac{4}{\pi\mu k^2} \begin{Bmatrix} -C_l^i \\ 2C_m^i \end{Bmatrix} \qquad \{q_i\} = \begin{Bmatrix} \frac{h_i}{b} \\ \alpha_i \end{Bmatrix}, \tag{38}$$

C_l^i is the lift coefficient for blade i and C_m^i is the moment coefficient about the elastic axis. The airfoil semi-chord is denoted by b, and μ is the airfoil mass ratio given by

$$\mu = \frac{m}{\pi \rho b^2}. \tag{39}$$

If the structural system (36) is written as a first order system

$$\dot{\overline{q}} = A_s \overline{q} + C_s y, \tag{40}$$

where $\overline{q} = (q \ \dot{q})^T$, then the coupled aerodynamic and structural system becomes

$$\left\{ \begin{array}{c} \dot{x} \\ \dot{\overline{q}} \end{array} \right\} = \overline{M}^{-1} \begin{bmatrix} A & \overline{B} \\ C_s C & A_s + C_s \overline{D} \end{bmatrix} \left\{ \begin{array}{c} x \\ \overline{q} \end{array} \right\}, \tag{41}$$

where $\overline{M}$ contains the coefficients of $\ddot{h}$ from the aerodynamic low order model and $\overline{B}$ and $\overline{D}$ are reduced forms of the matrices $\mathcal{B}$ and $\mathcal{D}$ which now multiply only displacement and velocity. At each timestep the structural and aerodynamic equations are solved simultaneously to determine the blade position, velocity and the aerodynamic forces and moments.

The eigenvalues of the coupled system (41) can be computed. For a plunge only case with $\omega_h = 10$ the eigenvalues are shown in figure 11. With such a stiff structure, we do not expect a lot of interaction between the flow and the structural dynamics. The original aerodynamic eigenvalues which were plotted in figure 6 are for the most part unmoved. We see the introduction of eight structural modes, all of which have a frequency of approximately ten, and varying amounts of aerodynamic damping from the righthand side term of equation (36). Considering now a case where the structure is more flexible, we see in figure 12 that for a structural frequency of $\omega_h = 1$ there is a greater movement of the original eigenvalues. Very lightly damped structural modes with frequencies around unity have been introduced.

The aerodynamic work per cycle is a measure of the energy transferred from the fluid to the structure in an oscillation period and is given by

$$W_h = \oint F.dh \tag{42}$$

for bending and

$$W_\alpha = \oint M.d\alpha \tag{43}$$

for torsion. These quantities can be used to assess the aeroelastic stability. If the work per cycle is positive, then there is a negative amount of damping being applied to the structure and the system is unstable. Negative but low in magnitude values of work per cycle indicate that a flow is lightly damped. A plot of aerodynamic work per cycle for this cascade is shown in figure 13. The work per cycle was computed for a number of different frequencies for interblade phase angles of $180°, 90°$ and $-90°$. This plot shows that the $\sigma = 90°$ case is very lightly damped for frequencies around unity. We can also see that the $-90°$ mode has positive damping for low frequencies around $\omega = 0.1$ indicating that the flow is unstable in this region. Figure 14 shows the system eigenvalues for a structural frequency of $\omega_h = 0.1$. We can see that, as expected from the work per cycle analysis, some of the lightly damped modes have crossed into the left half plane, indicating that the coupled system contains instabilities.

Simulations were run for the coupled system considering the cases with structural frequencies of 0.1 and 1. An initial plunge displacement was applied to one of the blades then the structural and aerodynamic response was computed. Figure 15 shows the resulting displacement and lift force for each blade for the $\omega_h = 1$ case. The displacements of the blades do die away, although this case is very lightly damped. Figure 16 shows the results for the $\omega_h = 0.1$ case. In this response we see that the system is unstable as expected from work per cycle and eigenvalue analysis.

Conclusions

Low order models offer many advantages for analysis of unsteady turbomachinery problems. Use of the frequency domain provides an efficient means of computing basis functions for these models, while development of the models in the time domain allows for ease of coupling to actuation and control models and provides a convenient framework for integration within more global engine models. The framework developed is particularly suited to the analysis of mistuned rotors where the interblade phase angles do not decouple and the entire rotor must be considered.

Good agreement with the linearised simulation code can be obtained with less than ten states per blade passage for each degree of freedom. The aerodynamic low order model is easily coupled to a simple structural model and can be used to compute system response to arbitrary disurbances. A model has been described here for pitching and plunging motions, however it is straightforward to include inlet and exit disturbances as additional model inputs.

Just the framework for development of these reduced order models has been described here. The technique is readily extended to viscous flows and to include multi-stage and three-dimensional analyses. More advanced models and applications will be discussed in follow-on papers.

References

[1]Crawley, E., "Aeroelastic Formulation for Tuned and Mistuned Rotors," AGARD Manual on Aeroelasticity in Axial-Flow Turbomachines Volume 2, 1988.

[2]Shapiro, B., "Mistuning Made Simple by Symmetry: An Analysis of Flutter Boundaries in Turbomachines," Working Paper C96-11-19, PRET, 1996.

[3]Whitehead, D., "Classical Two-Dimensional Methods," AGARD Manual on Aeroelasticity in Axial-Flow Turbomachines, Unsteady Turbomachinery Aerodynamics, Volume 1, 1987.

[4]Verdon, J., "Review of Unsteady Aerodynamic Methods for Turbomachinery Aeroelastic and Aeroacoustic Applications," *AIAA Journal*, Vol. 31, No. 2, February 1993, pp. 235–250.

[5]Hall, K., *A Linearized Euler Analysis of Unsteady Flows in Turbomachinery*, Ph.D. thesis, Dept. of Aeronautics and Astronautics, MIT, May 1987.

[6]Hall, K. and Florea, R., "A Reduced Order Model of Unsteady Flows in Turbomachinery," International Gas Turbine Congress and Exhibition, The Hague, The Netherlands, 1994.

[7]Sirovich, L., "Turbulence and the Dynamics of Coherent Structures. Part 1 : Coherent Structures," *Quarterly of Applied Mathematics*, Vol. 45, No. 3, October 1987, pp. 561–571.

[8]Willcox, K. E., *Aeroelastic Computations in the Time Domain Using Unstructured Meshes*, Master's thesis, Dept. of Aeronautics and Astronautics, MIT, February 1996.

[9]Wigton, L., Yu, N., and Young, D., "GMRES Acceleration of Computational Fluid Dynamics Codes," AIAA-85-1494, 1985.

[10]Giles, M., "Non-Reflecting Boundary Conditions for the Euler Equations," CFDL-TR 88-1, Massachusetts Institute of Technology, February 1988.

[11]Berkooz, G., Holmes, P., and Lumley, J., "The Proper Orthogonal Decomposition in the Analysis of Turbulent Flows," *Annual Review of Fluid Mechanics*, Vol. 25, 1993, pp. 539–575.

[12]Hall, K. and Silkowski, P., "The Influence of Neighboring Blade Rows on the Unsteady Aerodynamic Response of Cascades," ASME 95-GT-35, 1995.

[13]Dugundji, J. and Bundas, D., "Flutter and Forced Response of Mistuned Rotors Using Standing Wave Analysis," *AIAA Journal*, Vol. 22, No. 11, November 1984, pp. 1652–1661.

[14]Hall, K., "Eigenanalysis of Unsteady Flows About Airfoils, Cascades and Wings," *AIAA Journal*, Vol. 32, No. 12, December 1994, pp. 2426–2432.

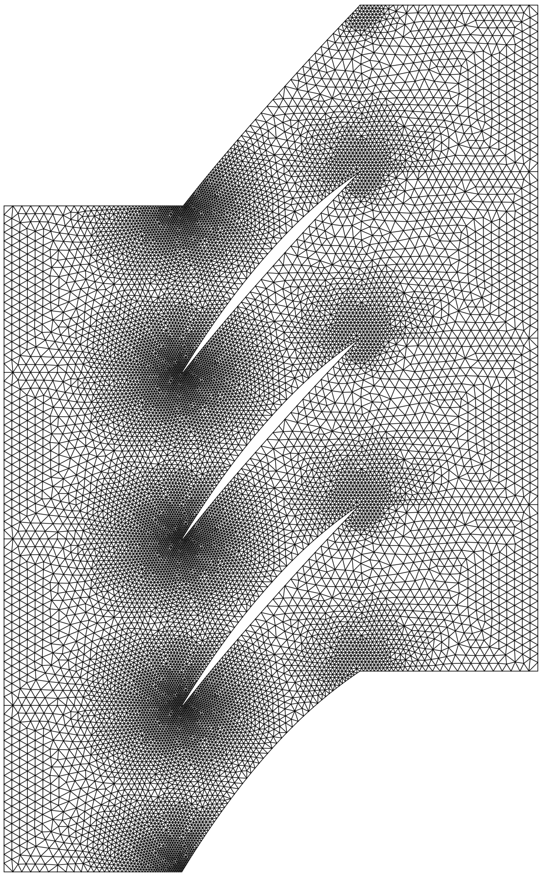

Fig. 2 Computational domain for four passage DFVLR transonic rotor. 14459 nodes, 28160 triangles.

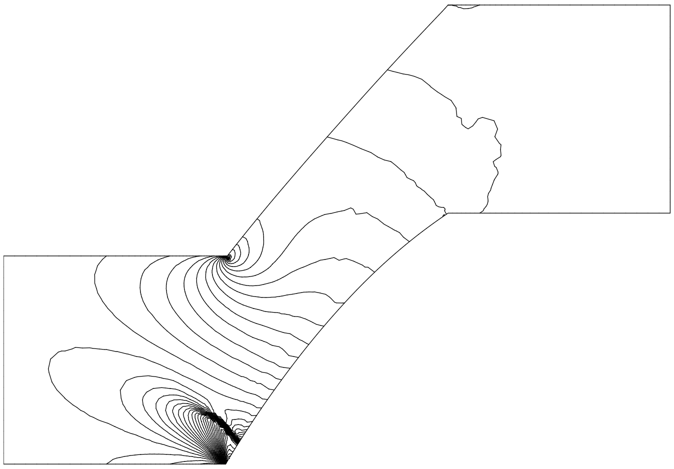

Fig. 3 Pressure contours for steady inviscid transonic flow. $M = 0.82$, $\alpha = 58.5°$

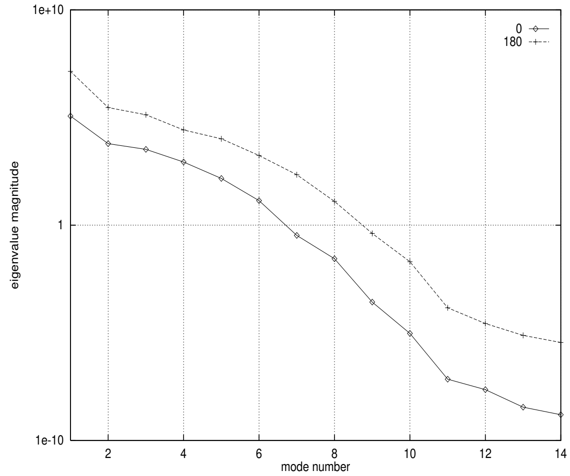

Fig. 4 Eigenvalue spectra for POD analyses of transonic cascade in plunge. $M = 0.82, \sigma = 0°, 180°$

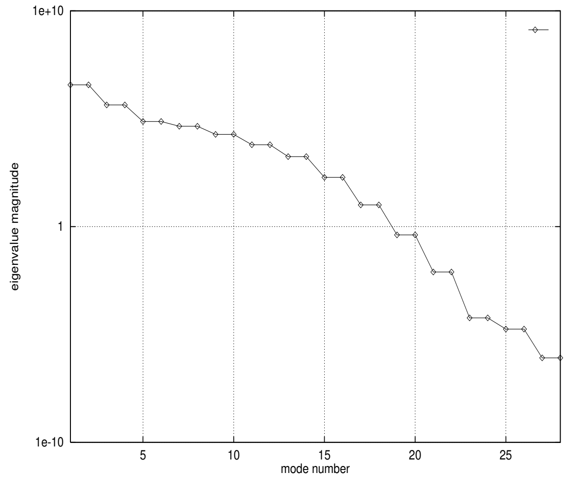

Fig. 5 Eigenvalue spectra for POD analyses of transonic cascade in plunge. $M = 0.82, \sigma = \pm 90°$

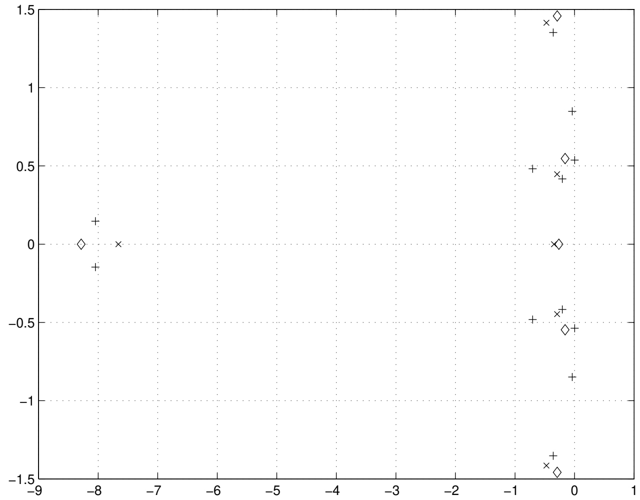

Fig. 6 Eigenvalue spectrum for low order aerodynamic system. Six modes per interblade phase angle. $M = 0.82$, $\sigma = 0°$ **(crosses),** $180°$ **(diamonds),** $\pm 90°$ **(plus signs).**

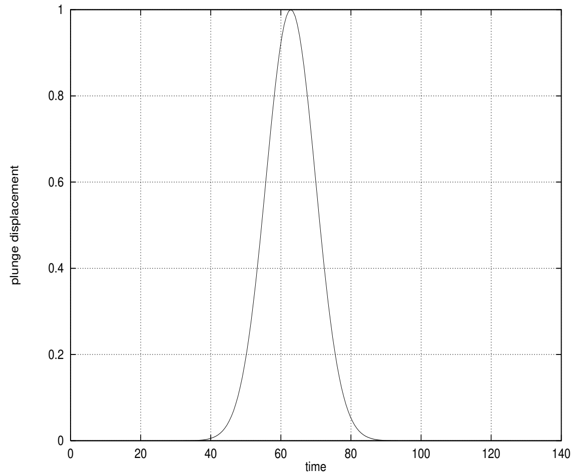

Fig. 7 Pulse input in plunge.

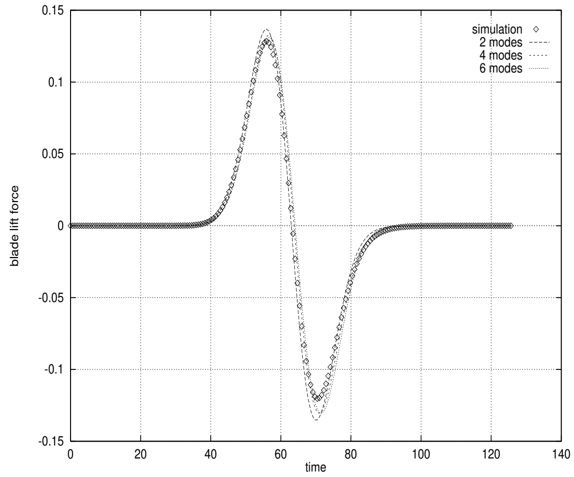

Fig. 8 Pulse response for low order model and linearised simulation code. $\sigma = 0°$, $g = 0.01$, $M = 0.82$

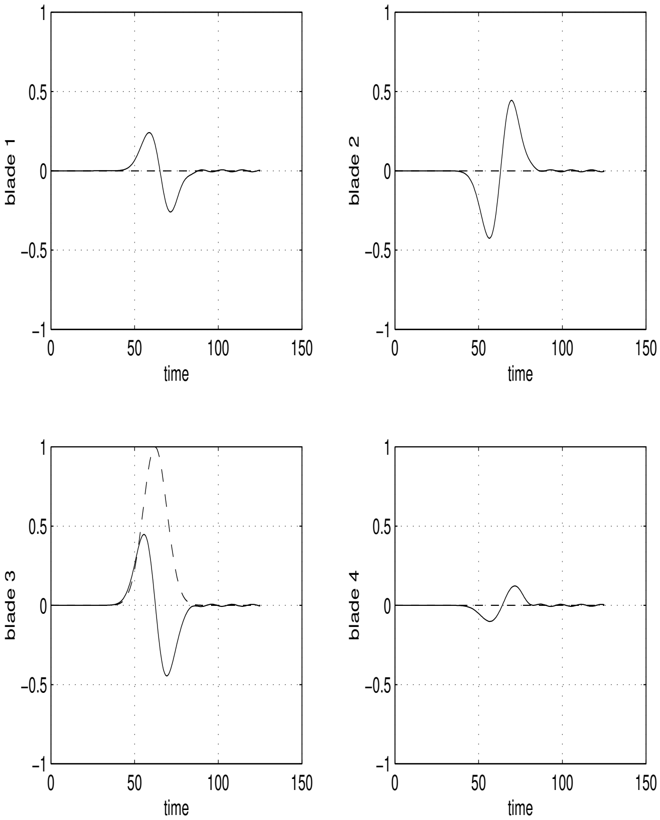

Fig. 9 Pulse displacement input (dashed line) and blade lift force response (solid line) for low order model. Six modes per interblade phase angle. $g = 0.01$, $M = 0.82$

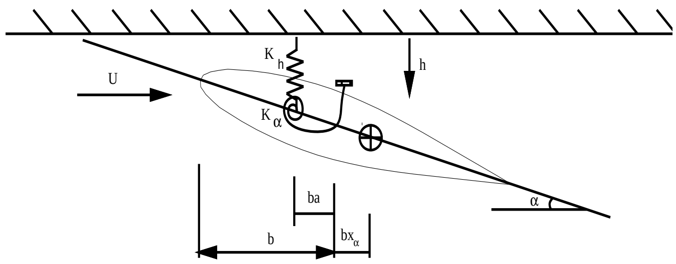

Fig. 10 Typical section structural model for blade i**.**

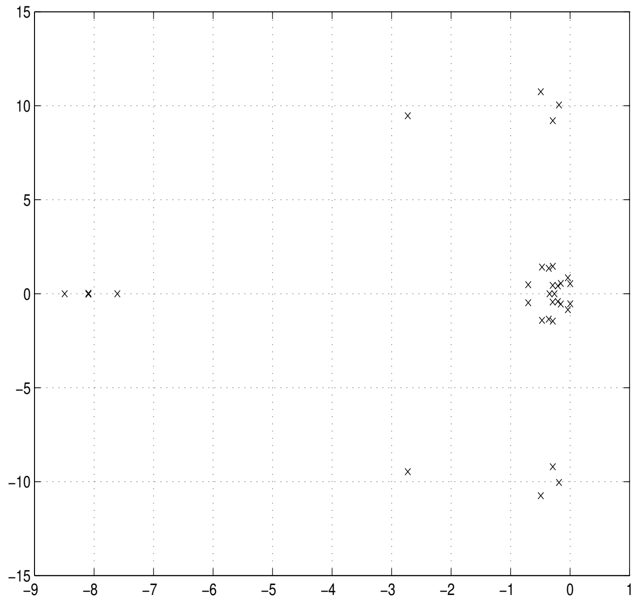

Fig. 11 Eigenvalue spectrum for coupled system. Six modes per interblade phase angle. $M = 0.82$, $\mu = 60$, $\omega_h = 10$.

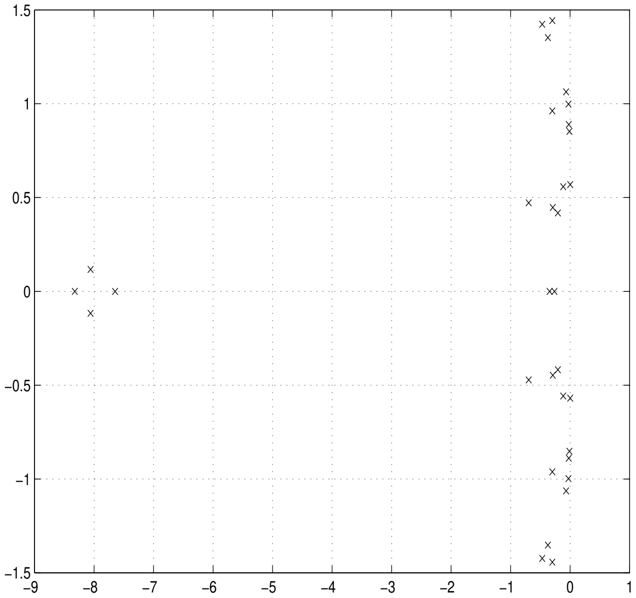

Fig. 12 Eigenvalue spectrum for coupled system. Six modes per interblade phase angle. $M = 0.82$, $\mu = 60$, $\omega_h = 1$.

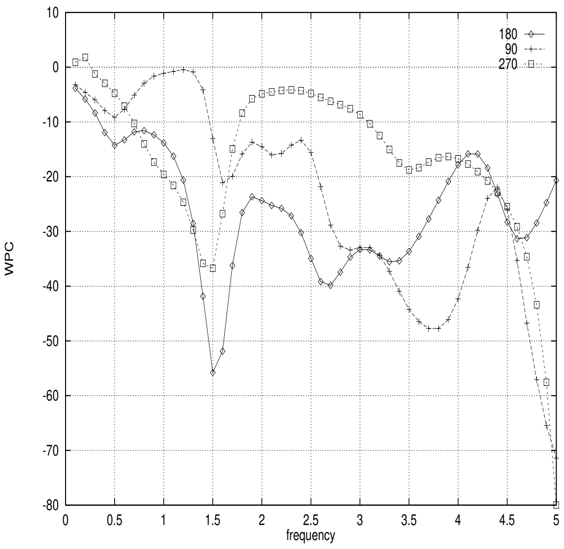

Fig. 13 Aerodynamic work per cycle as a function of frequency for $\sigma = 180°, 90°, -90°$

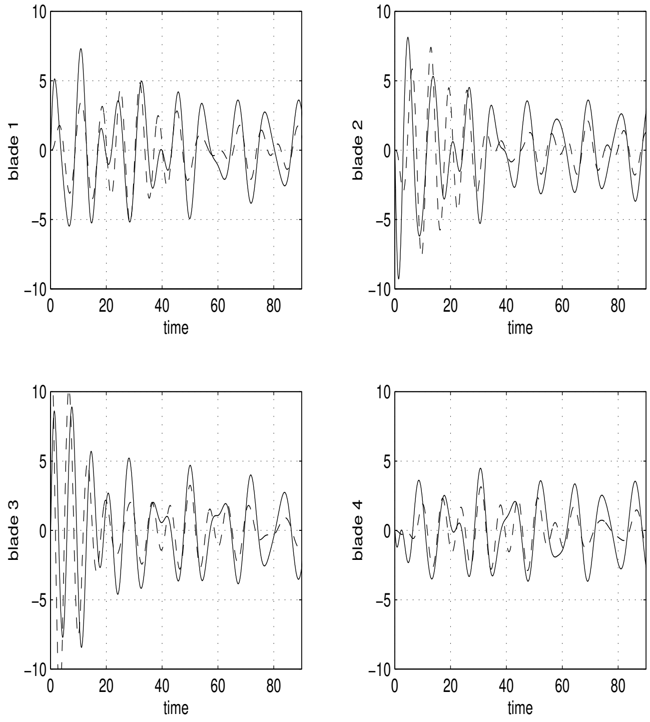

Fig. 15 Response to a plunge displacement input at blade 3 : blade displacement (dashed line) and blade lift force (solid line). Six modes per interblade phase angle. $M = 0.82$, $\mu = 60$, $\omega_h = 1$.

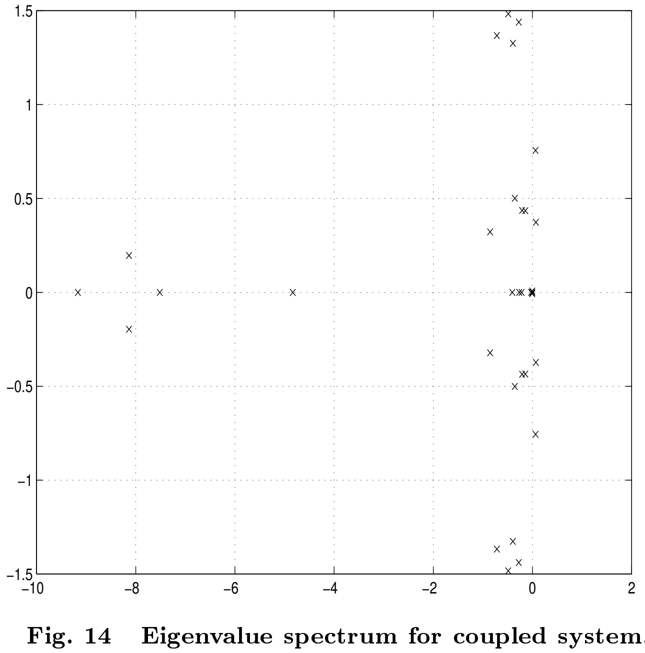

Fig. 14 Eigenvalue spectrum for coupled system. Six modes per interblade phase angle. $M = 0.82$, $\mu = 60$, $\omega_h = 0.1$

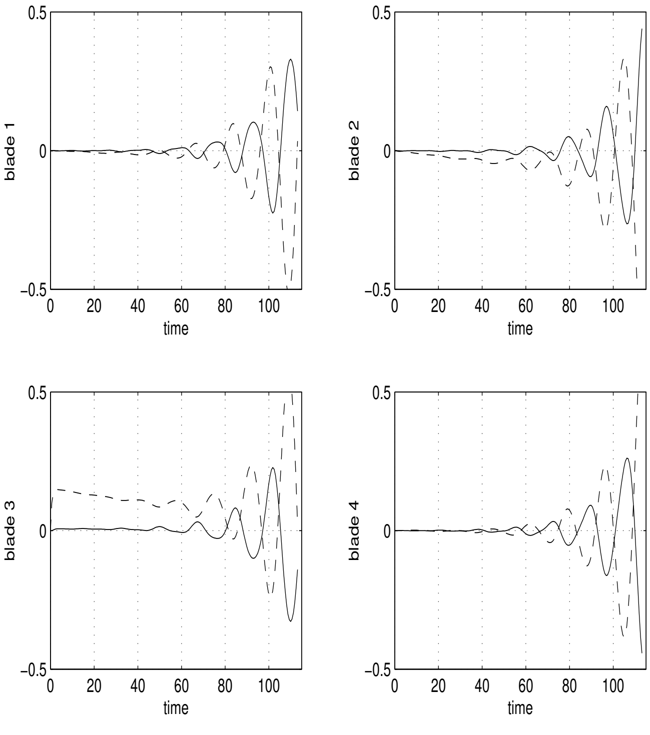

Fig. 16 Response to a plunge displacement input at blade 3 : blade displacement (dashed line) and blade lift force (solid line). Six modes per interblade phase angle. $M = 0.82$, $\mu = 60$, $\omega_h = 0.1$